Supporting Information

Intensity Ratio of Resonant Raman Modes for (*n,m*) Enriched Semiconducting Carbon Nanotubes

Yanmei Piao, [a] Jeffrey R. Simpson, [a, b] Jason K. Streit, [c] Geyou Ao, [c] Ming Zheng, [c]

Jeffrey A. Fagan, [c]* Angela R. Hight Walker [a]*

*Corresponding email: angela.hightwalker@nist.gov, jeffrey.fagan@nist.gov

[a] Physical Measurement Laboratory, National Institute of Standards and Technology
Gaithersburg, Maryland
[b] Department of Physics, Astronomy and Geosciences, Towson University
Towson, Maryland
[c] Material Measurement Laboratory, National Institute of Standards and Technology
Gaithersburg, Maryland

Contents

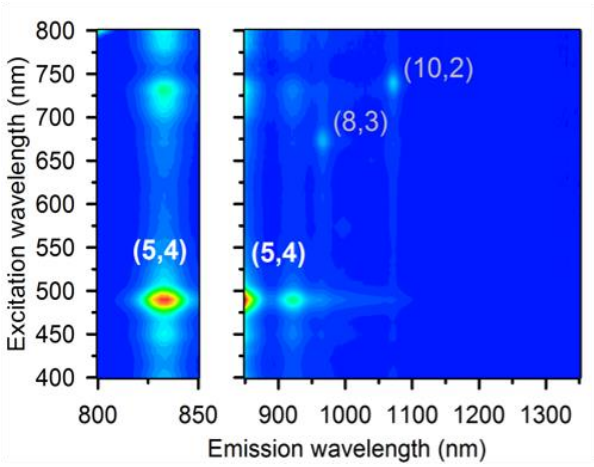

Figure S1. PL map of (5,4)* sample acquired with silicon PMT (left) and InGaAs (right) array detector. The * denote that the sample is enriched in (5,4) with other minor species.

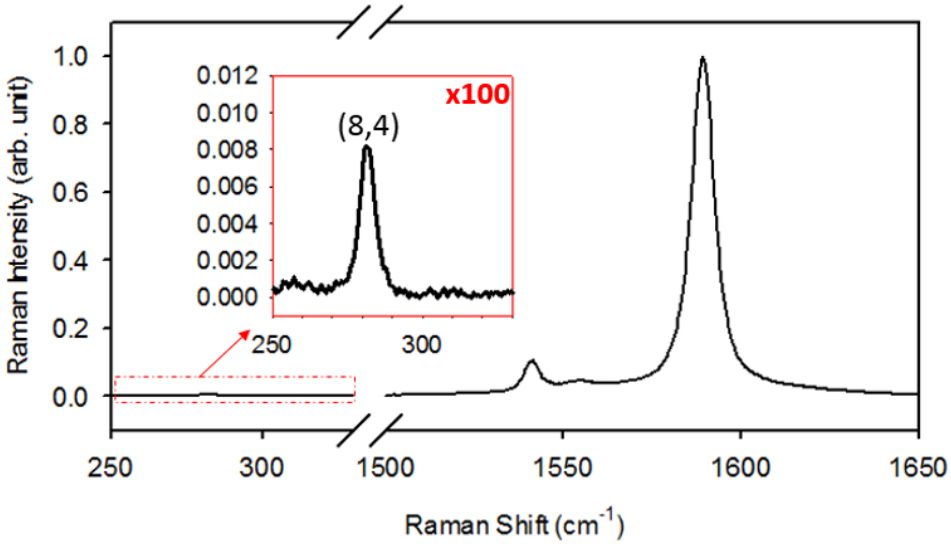

Figure S2. (8,4) resonance Raman spectrum collected using 597 nm excitation which is the E_{22} value determined from the absorption spectrum. Inset figure shows the RBM of (8,4) enlarged by two orders of magnitude.

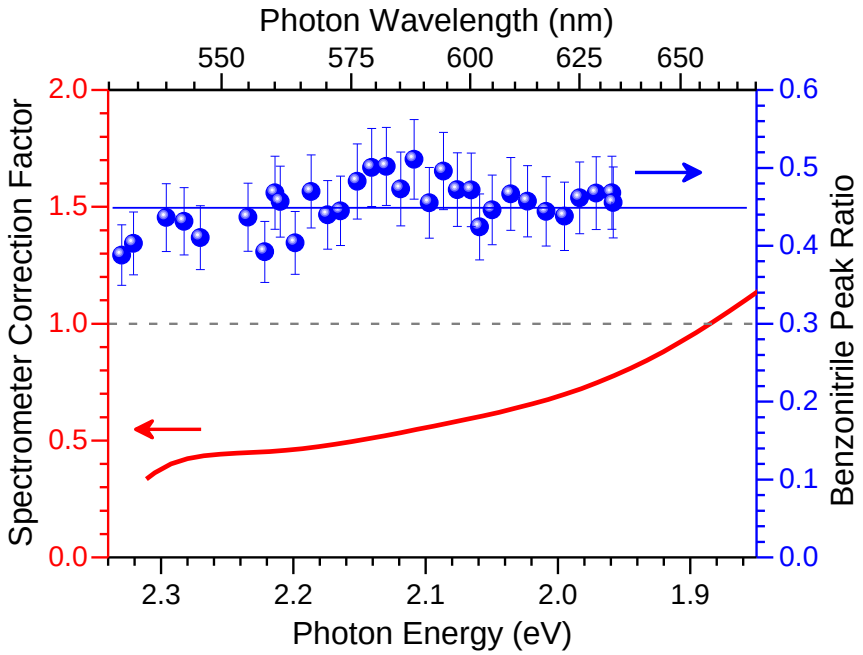

Figure S3. Spectrometer intensity correction factor shown in red (left axis) as a function of photon excitation energy (bottom axis) over the range of SRMs to the lower energy limit used in this work. Blue dots represent the ratio of integrated areas for the Raman-active benzonitrile peaks at 460.9 cm^{-1} to 1598.9 cm^{-1} (right axis) versus the excitation wavelength (top axis) after application of the intensity correction factor. Solid blue line indicates the average value of the corrected benzonitrile peak area ratios. The error bar (10%) for each data point is estimated from fluctuations in the laser power.

Table S1. Value of I_{RBM} (using E_{22} excitation) extracted from tabulated data in reference 1.

Dominant (*n*,*m*)	**Intensity of RBM (arb. unit) under E_{22} excitation**
(5,4)	845
(6,4)	3515
(7,3)	136
(6,5)	516
(8,3)	5311
(10,0)	2336
(9,2)	1267
(7,5)	2165
(8,4)	84
(7,6)	292
(11,1)	1936

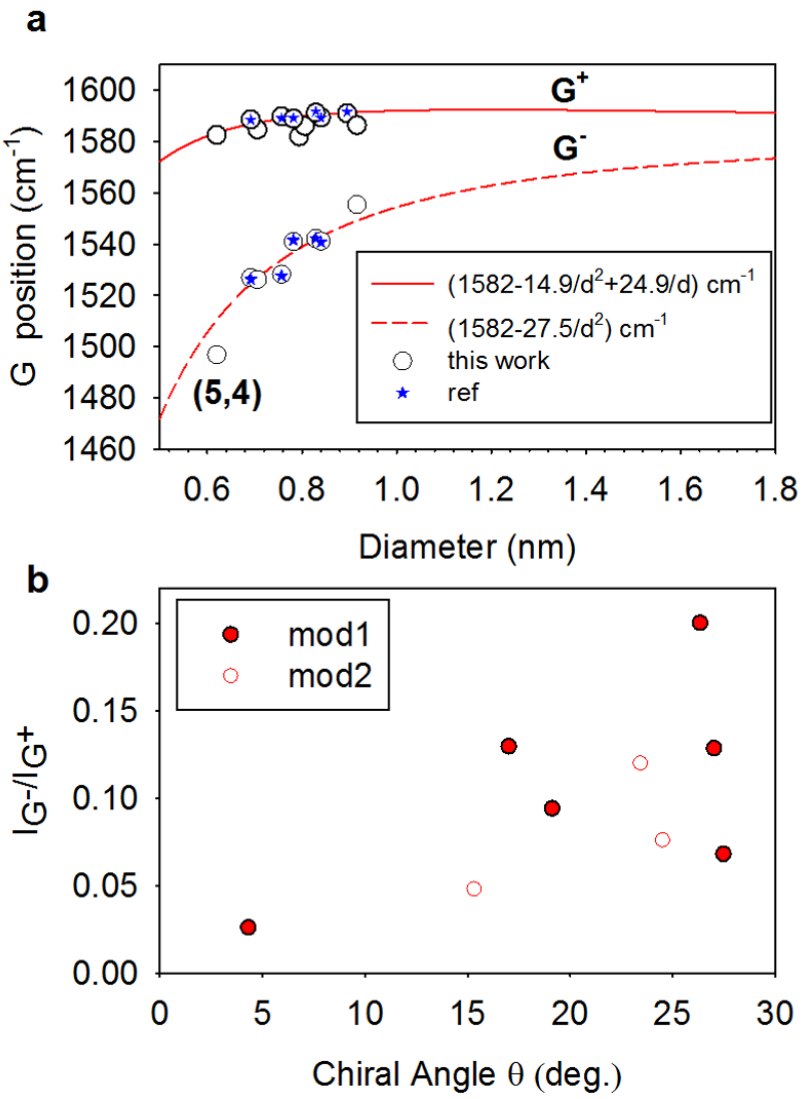

Figure S4. (a) G^- and G^+ position *vs* diameter of different SWCNTs. The red lines are generated from the equations shown in the inset,[2] the black circles are the data observed in this work, and the blue stars are reported values from reference 2. (b) Intensity ratio of G^- to G^+ *vs.* chiral angle of different SWCNTs.

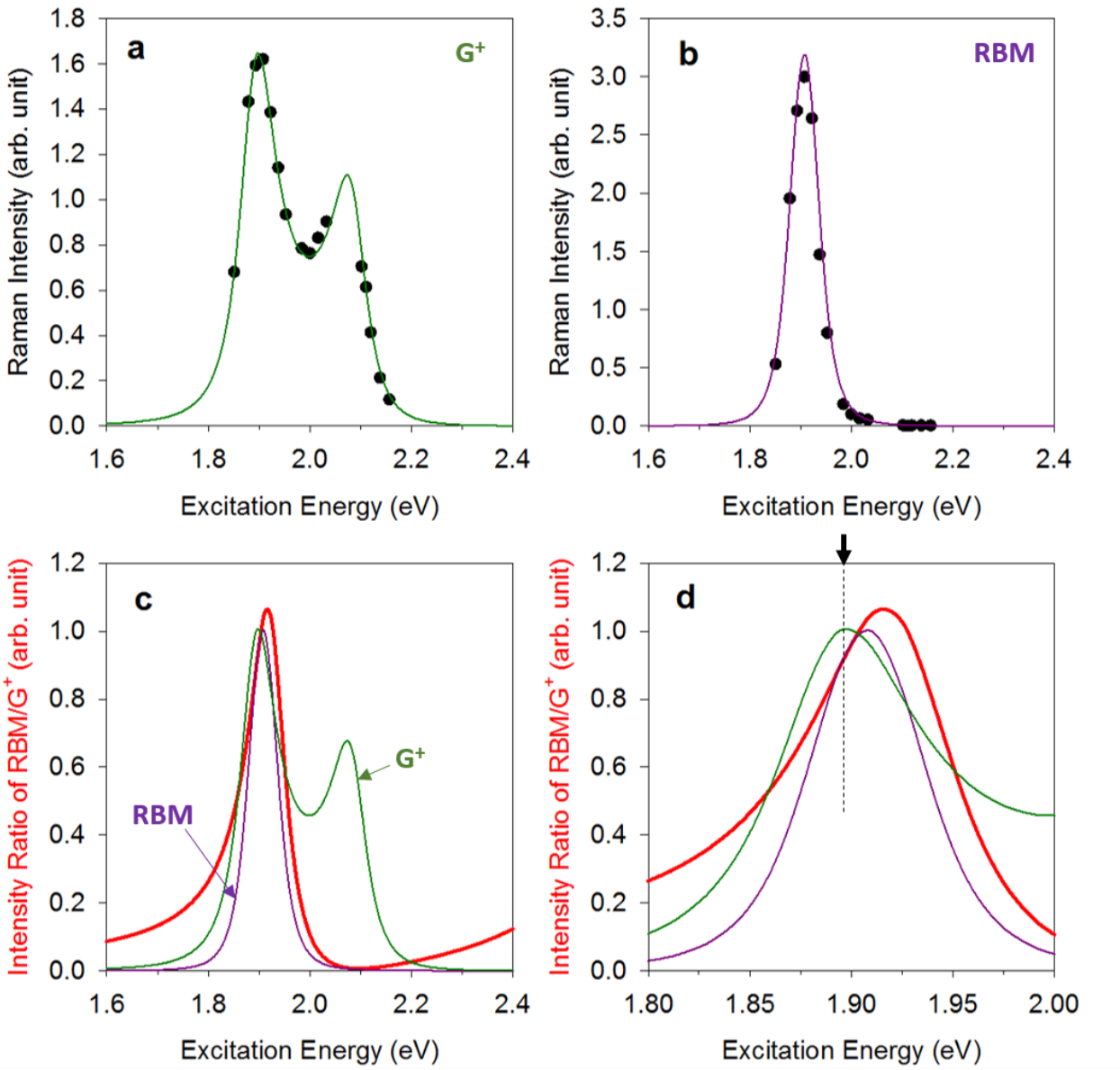

Figure S5. Full REP of **(a)** G^+ and **(b)** RBM of (7,5). The dots are experiment data points and the colored curves, green for G^+ and purple for RBM, are fitted results. Equation S1 was used to fit the data. **(c)** Fitted REP of G^+ (green) and RBM (purple) are normalized to one and the ratio of the two are plotted as the red line. **(d)** The incoming resonance part in **(c)** was enlarged. The arrow indicates the excitation energy which is used to determine the RBM/G^+ intensity ratio reported in Table 1. The maximum of the ratio should appear at a slightly higher energy than at the excitation energy, which is consistent with our experiment observation.

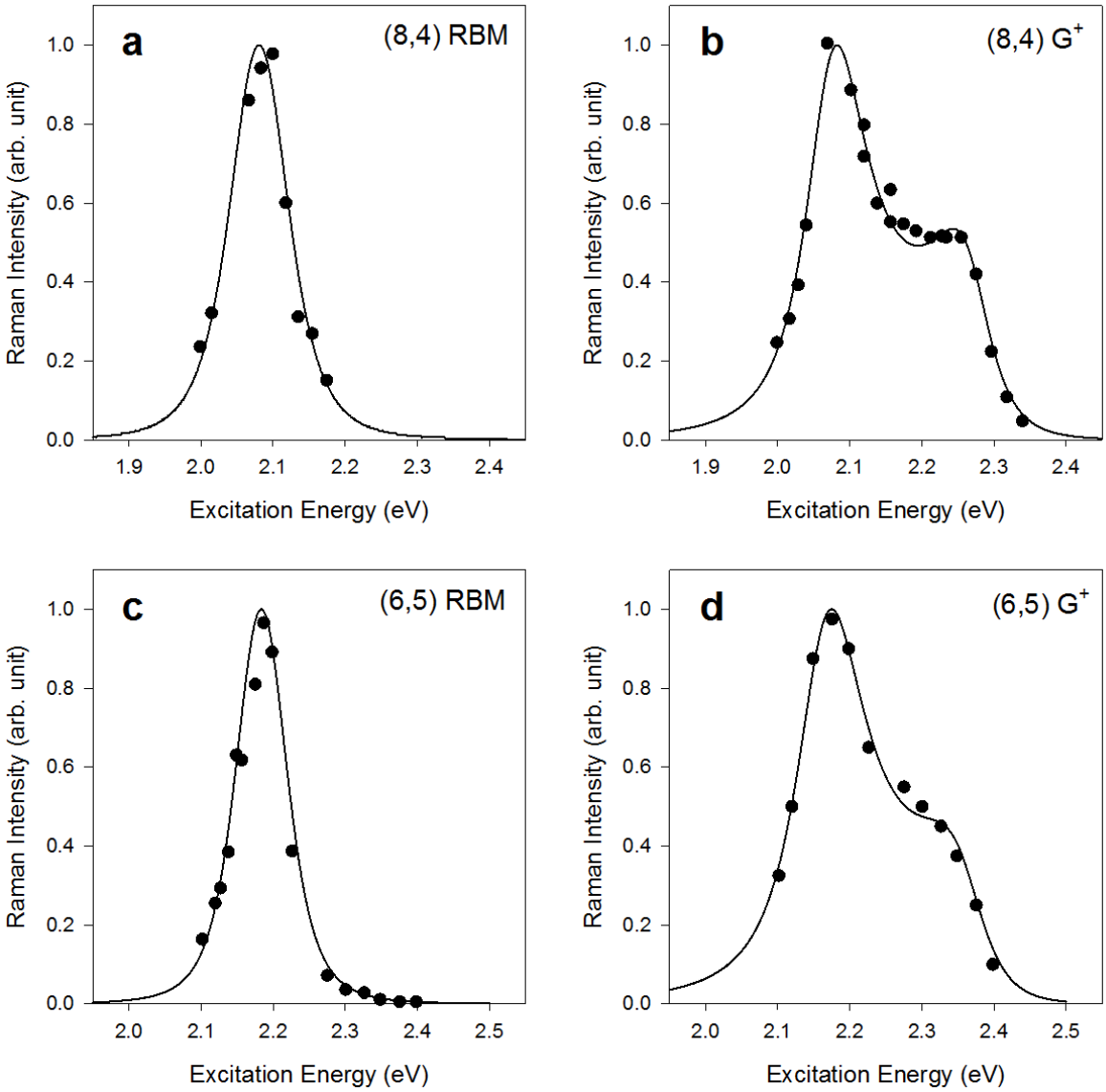

Figure S6. (a,b) Full REP of (8,4) RBM and G^+. **(c,d)** Full REP of (6,5) RBM and G^+. The dots are experiment data and the lines are fitted following the Equation S1. All the spectra are normalized to one.

Description of broadening factor Γ *within* an (*n,m*)

Both the incoming and outgoing resonances contribute to the RBM and G^+ REP intensity at E_{22}. Moreover, the incoming and outgoing resonance contributions can vary given not only the differences in energy of the RBM and G^+ modes and the asymmetry of the G^+ REP, but also the broadening term, Γ. In order to more fully assess these contributions, we have completed Raman REPs (RBM and G^+) on (8,4), (6,5) and (7,5) in Fig. S5 and Fig. S6, along with the corresponding analysis and modeling. Equation S1 and S2 were used for REP fitting.[3]

During the analysis, we assumed a constant REP broadening factor (Γ) for both the RBM and G^+ *within the same chirality*. Our assumption is based on literature[3,4] and our experiment results. In Table S2 we show that the variation of Γ-RBM to Γ-G^+ within a specific chirality is relatively small for (7,5) and (6,5) (% difference of 5 % and 12 %, respectively) which supports the assumption. However, in the case of the (8,4), the difference between the Γ-RBM and Γ-G^+ is larger (~25 %). Of note, the extremely low signal strength of the (8,4) RBM results in a higher uncertainty for each experimental data point and thus leads to a higher uncertainty in the REP fitting used to determine Γ-RBM. In summary, the literature and our experimental results generally support the assumption that REP broadening factors are *similar* for RBM and G^+ *within the same chiral species*.

Equations used to fit the REPs

$$I \propto \left| \frac{M_1}{E_L - E_{22} - i\frac{\Gamma}{2}} + \frac{M_2}{E_L - E_{22} - E_{ph} - i\frac{\Gamma}{2}} \right|^2$$

Equation S1

$$C = \frac{M_1 + M_2}{M_1 - M_2}$$

Equation S2

Where

I = Raman intensity (arb. unit)
C = non-Condon parameter
M_1 = the matrix elements for both the absorption and emission processes of the exciton-photon interaction, as well as for the exciton-phonon coupling of incoming resonance
M_2 = the matrix elements for both the absorption and emission processes of the exciton-photon interaction, as well as for the exciton-phonon coupling of outgoing resonance
E_L = laser excitation energy (eV)
E_{22} = the second electronic transition energy (eV)
E_{ph} = phonon energy (eV)
Γ = broadening term (eV)

Table S2. REP fitting parameters

(*n,m*)	E_{22} / eV		Γ / meV		M_1		C
	RBM	G^+	RBM	G^+	RBM	G^+	
(7,5)	1.886	1.889	81 ± 2	91 ± 2	0.0688	0.0592	0.12
(6,5)	2.164	2.165	114 ± 7	120 ± 7	0.0693	0.0860	0.26
(8,4)	2.063	2.073	138 ± 9*	106 ± 4	0.0145	0.0772	0.19

* The Γ value of (8,4) RBM and the associated error are significantly larger than that of its G^+ compared with the other two chiralities shown here. This effect is likely due to the extremely low RBM signal of (8,4) through the resonance window.

Description of effects of varying parameters (Γ and *C* values, Raman mode frequencies) on RBM/G^+ ratio

We used our data to approximate the variance of Γ-RBM and Γ-G^+ and then modeled the REPs using Equation S1 on the intensity ratio at E_{22}. Our full REPs yield Γs that vary by approximately +/-19% between chiralities (Table S2). A similar variance in the Γ of E_{22} excitation was measured from the photoluminescence excitation (PLE) spectra of all 11 (*n,m*)s shown in Fig. 1(c) and Fig S1. This observed Γ variance could affect the intensity ratio by at worst 25% as seen in the curve for Fig. S7 (a).

The degree to which variations in the frequency of G^+ and RBM could affect the overlap of the outgoing resonance and hence the RBM/G^+ intensity ratio at E_{22} was also assessed. The small variation in the G^+ frequency, from our data specifically (1583 cm^{-1} and 1591 cm^{-1}), results in a negligible contribution to the intensity ratio (< 0.1%) as seen in Fig. S7 (d). The larger variation in the RBM frequency across the range of our 11 SWCNTs (259 cm^{-1} to 372 cm^{-1}), however, results in a correspondingly larger effect (~+/- 15%) on the E_{22} intensity ratio as seen in Fig. S7 (b).

Finally, we examined the effect of the asymmetry of the outgoing resonance on the G^+ REP, as quantified by the non-Condon parameter *C* on the RBM/G^+ intensity ratio.[5] Changing *C* from 0 to 0.5, which is much larger than both our measured values (Table S2) and the typical range reported for multiple semiconducting SWCNTs[5] did not affect appreciably the intensity ratio (< 2.5%) as seen in Fig. S7 (c).

Our analysis of the effect of various incoming and outgoing resonance parameters on the intensity ratio of RBM/G^+ reveals that variations in the broadening factor Γ and the RBM frequency provide the largest effects. The RBM frequencies were measured (see Table 1) and correction for their variance is straightforward. In the absence of Γ values from Raman REPs for all 11 (*n,m*)s, we used the Γs from our PLE data, scaled appropriately to coincide with the three measured Raman Γ values. The resulting correction factors from both the RBM frequencies and the Γs have been applied to the intensity ratios and are shown in Fig. S8. Furthermore, from fitting the three full REPs, we obtain the incoming resonance matrix elements M_1 and plot the ratio squared $[|M_{1,\ RBM}|^2/|M_{1,\ G+}|^2]$ on the same figure. These plots all follow the theoretical

prediction and agree with the intensity ratio determined at E_{22} further validating the use of this technique.

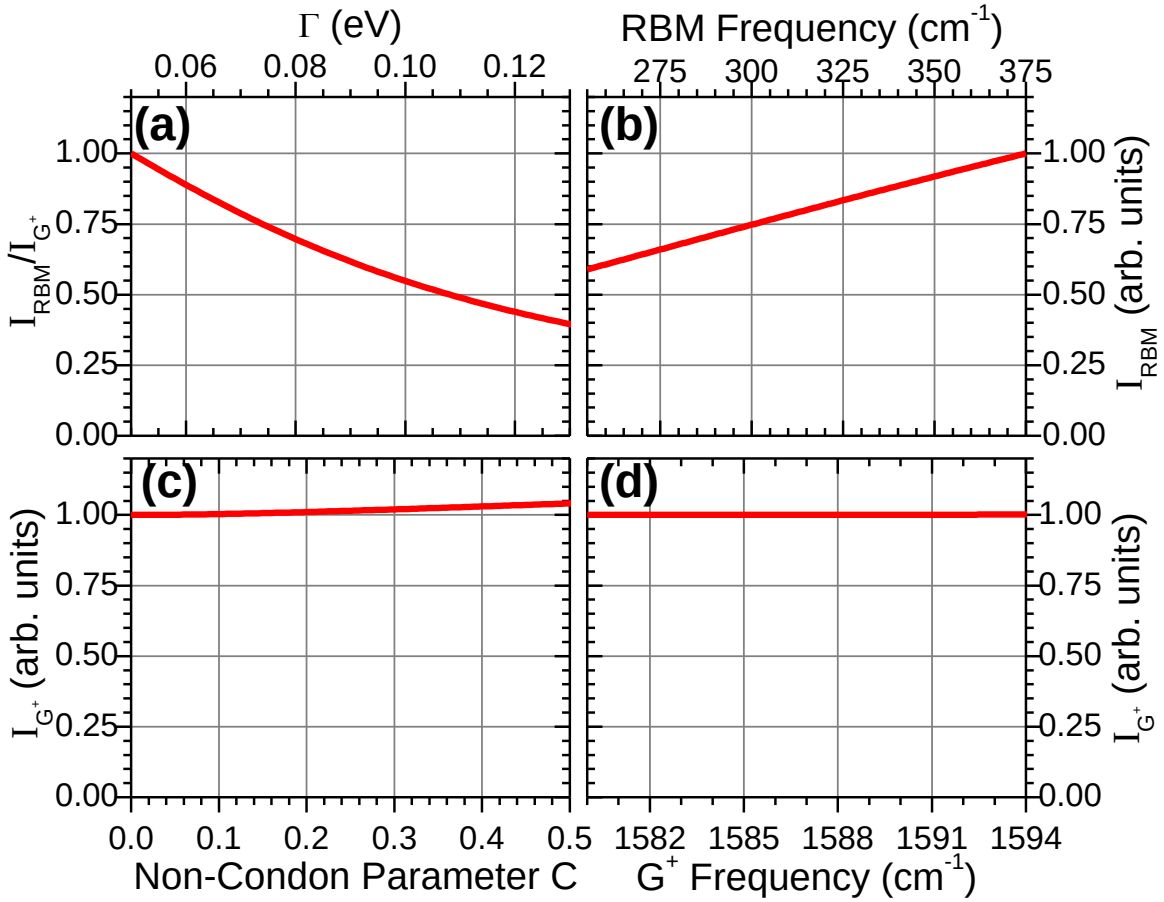

Figure S7. Results of modeling the effects of indicated parameters on the RBM/G^+ intensity ratio, intensity of RBM, and intensity of G^+ at E_{22} excitation: **(a)** Intensity ratio of RBM/G^+ *vs.* broadening factor Γ (eV), **(b)** Intensity of RBM *vs.* frequency of the RBM phonon, (c) Intensity of G^+ *vs.* non-Condon parameter *C*, and **(d)** Intensity of the G^+ *vs.* frequency of the G^+ phonon. Vertical axes are plotted in arbitrary units scaled to unity.

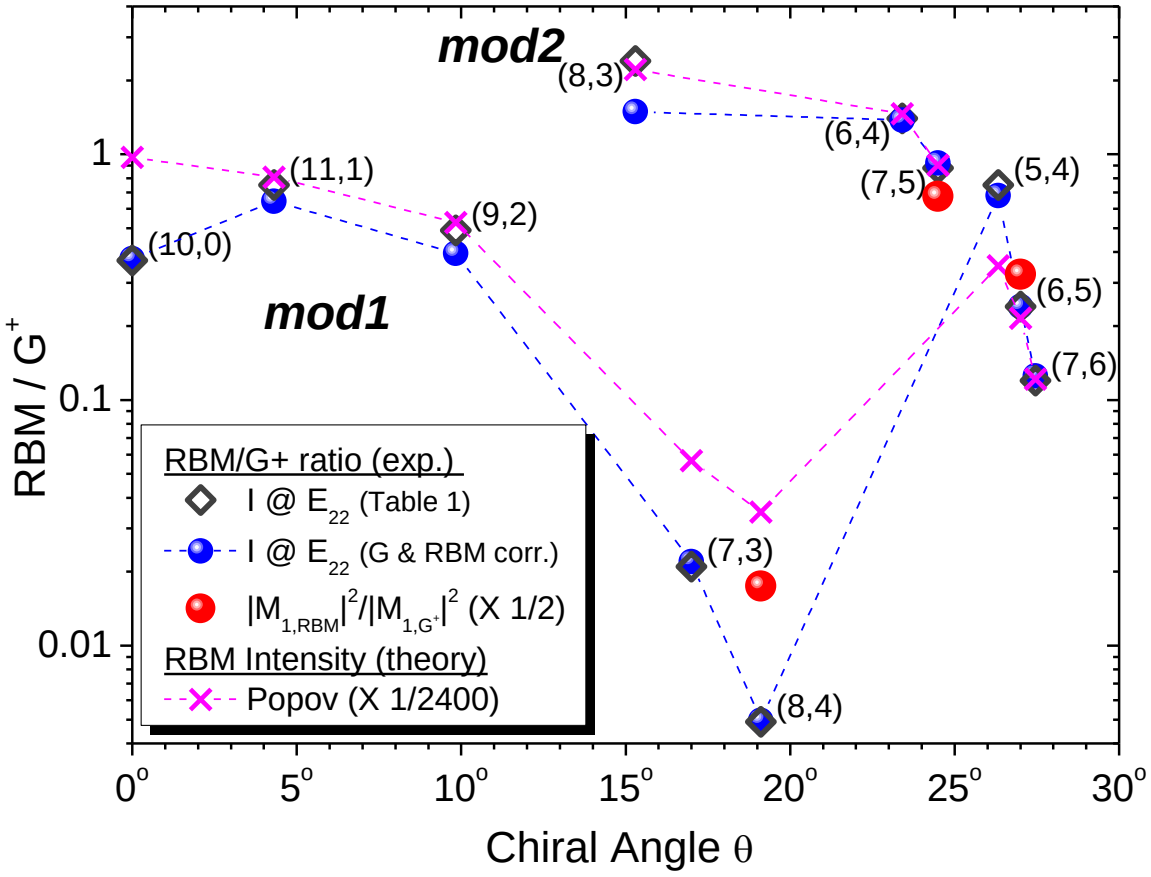

Figure S8. RMB/G^+ intensity ratios (log scale) as a function of chiral angle θ for SWCNT (*n,m*)s as labeled. Mod1 and mod2 appear in the lower and upper halves of the figure, respectively, with dashed lines to guide the eye. Experimental RBM/G^+ intensity ratios obtained at E_{22} excitation as reported in Table 1 and those values corrected for RBM and G are shown as open black diamonds and filled blue circles, respectively. Red circles represent the values of [$|M_{1,RBM}|^2/|M_{1,G+}|^2$] (scaled by x1/2) for (8,4), (7,5) and (6,5) derived from full REPs. Pink crosses represent the predicted RBM intensities (scaled by x1/2400) from Popov *et al.*[1]

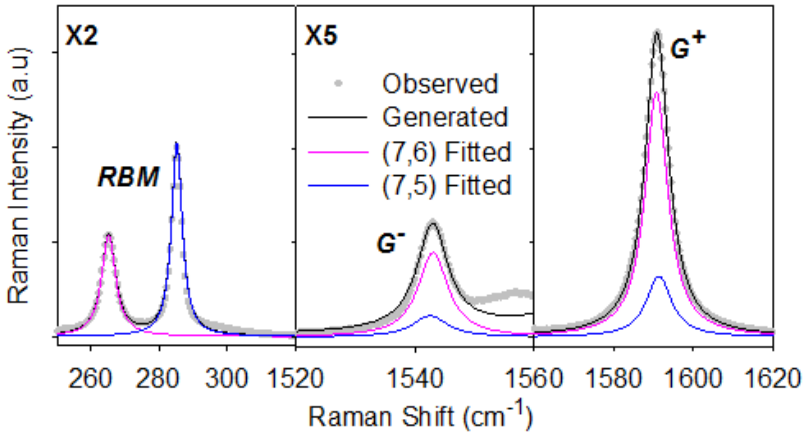

Figure S9. G^- and G^+ modes of (7,6) derived from spectra decoupling process from (7,6)* Raman spectrum using RBM intensity as an internal reference.

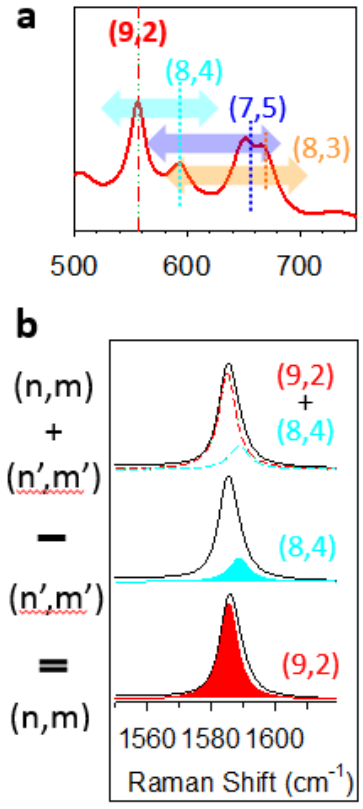

Figure S10. (a) Absorption spectrum of (9,2)* at E_{22} region. The G resonance window of the minor species are indicated with double side arrows. From the figure we can see only (8,4) will contribute to the G^+ peak of (9,2)*. (b) Decoupling process shows how to subtract the (8,4) contribution from (9,2)* spectrum and isolate the (9,2) G^+ peak.

References

(1) http://www.phys.uni-sofia.bg/~vpopov/cnts.htm.

(2) Telg, H.; Duque, J. G.; Staiger, M.; Tu, X.; Hennrich, F.; Kappes, M. M.; Zheng, M.; Maultzsch, J.; Thomsen, C.; Doorn, S. K. Chiral Index Dependence of the G^+ and G^- Raman Modes in Semiconducting Carbon Nanotubes. *ACS Nano* **2012**, *6*, 904–911.

(3) Hároz, E. H.; Duque, J. G.; Barros, E. B.; Telg, H.; Simpson, J. R.; Hight Walker, A. R.; Khripin, C. Y.; Fagan, J. A.; Tu, X.; Zheng, M.; *et al.* Asymmetric Excitation Profiles in the Resonance Raman Response of Armchair Carbon Nanotubes. *Phys. Rev. B* **2015**, *91*, 205446.

(4) Hároz, E. H.; Duque, J. G.; Rice, W. D.; Densmore, C. G.; Kono, J.; Doorn, S. K. Resonant Raman Spectroscopy of Armchair Carbon Nanotubes: Absence of Broad G-Feature. *Phys. Rev. B* **2011**, *84*, 121403.

(5) Duque, J. G.; Chen, H.; Swan, A. K.; Shreve, A. P.; Kilina, S.; Tretiak, S.; Tu, X.; Zheng, M.; Doorn, S. K. Violation of the Condon Approximation in Semiconducting Carbon Nanotubes. *ACS Nano* **2011**, *5*, 5233–5241.